Journal of Quantitative Spectroscopy & Radiative Transfer 111 (2010) 1262–1276

Contents lists available at ScienceDirect

Journal of Quantitative Spectroscopy & Radiative Transfer

journal homepage: www.elsevier.com/locate/jqsrt

Water dimer vibration–rotation tunnelling levels from vibrationally averaged monomer wavefunctions

Ross E.A. Kelly [a], Jonathan Tennyson [a,*], Gerrit C. Groenenboom [b], Ad van der Avoird [b,*]

[a] Department of Physics and Astronomy, University College London, London WC1E 6BT, UK
[b] Theoretical Chemistry, Institute for Molecules and Materials, Radboud University, Nijmegen, Heyendaalseweg 135, 6525 AJ Nijmegen, The Netherlands

ARTICLE INFO

Article history:
Received 21 November 2009
Received in revised form
26 January 2010
Accepted 27 January 2010

Keywords:
Water dimer
Transition wavenumbers
Atmospheric physics
Water continuum

ABSTRACT

The vibration–rotation tunnelling (VRT) spectra for the water dimer obtained by vibrationally averaging the dimer potential over accurate water monomer wavefunctions is reported. The vibrational averaging requires evaluation of the 12D dimer potential energy surface at more than 10^{12} distinct geometries. The resulting vibrational spectra of the low-lying dimer states are presented and compared with both less computationally expensive methods based on fixed nuclei approximations and the recent (6+6)*d* adiabatic calculations of Leforestier et al. [38] (2009). The procedure gives some modest improvement in the agreement with experimental values for the vibration–rotation tunnelling (VRT) states of $(H_2O)_2$ and $(D_2O)_2$. This approach can be extended to treat dimer states involving monomer overtone excitations, which is important in obtaining water dimer spectra at infrared and visible wavelengths at atmospheric temperatures, and in characterizing the dimer contribution to the so-called water continuum absorption at these wavelengths.

1. Introduction

The water molecule is one of the most simple and important molecules in nature. However, the molecule has unusual properties which make many characteristics difficult to investigate theoretically. Research into water is wide ranging: from the simulation of liquid water and ice [1–5], to small water clusters [6,7] and spectroscopy. The latter is extremely important in both our understanding of the Earth's atmosphere and that of extra-terrestrial bodies [8,9]. One question which remains unresolved is whether there is a contribution from water dimer to the water vapour continuum absorption spectrum in the atmosphere. Experimental evidence in small spectroscopic regions suggest that the dimer contribution is possible [10–12]. However, this may simply be an artefact of the monomer absorption [13], or the far wing hypothesis [14], or even other collision-induced absorption [15–17].

Theoretical understanding of the water dimer problem at solar radiation wavelengths is difficult since a direct solution of the full 12D nuclear motion problem for the water dimer problem is not currently feasible. Therefore, theoretical work in this area relies on approximations which make the calculations tractable. Examples include the MULTIMODE approach of Bowman and co-workers [18] or the harmonically coupled anharmonic oscillator (HCAO) methods of Kjaergaard et al. [19–24]. The latter studies provide evidence which suggests, in particular, that the OH stretching fundamentals and overtones of the water dimer contribute to the water continuum spectra [15,16,22–24]. To improve our current theoretical understanding of the water dimer spectroscopy, both new spectroscopic methods and development of a highly accurate water dimer potential surface are required.

Theoretical studies based on the rigid dimer Hamiltonian of Brocks et al. [25] have been used extensively for investigating the far infrared spectral region [26–28].

* Corresponding authors.
E-mail address: j.tennyson@ucl.ac.uk (J. Tennyson).

0022-4073/$ - see front matter © 2010 Elsevier Ltd. All rights reserved.
doi:10.1016/j.jqsrt.2010.01.033

Most work in this area has studied the low lying states which are probed in low temperature experiments [1,28–38]. A crucial factor in these calculations is the accuracy of the (6D) water dimer potential. One of the most reliable tests of the accuracy of a dimer surface is its ability to reproduce the tunnelling splittings of the water (and D_2O) dimer which have been observed with high resolution microwave and far-infrared spectroscopy [39–45,31,30].

Development of a 12D flexible water dimer potential energy surface (PES) is an important step in creating accurate water dimer spectra. There are many characteristics that the water dimer surface should contain [46–50] which makes development of a good dimer potential difficult. However, much progress has been made in this area with the construction of fully ab initio 6D CCpol potentials of Szalewicz et al. [1,35–37] and 12D potentials of Huang et al. [51,28]. The advantage of the fully flexible nature of the 12D potentials is that they may be used for *full dimensional* calculations on the water dimer [18]. However, when compared to the CCpol 6D set of potentials they have a lower relative grid coverage. The CCpol potentials also include an extrapolation to the complete basis set (CBS) limit and additional sites in the potential expression which systematically improve the accuracy of the potentials when compared to experiment. We note that the original Huang et al. potentials (HBB0 and HBB) were found to reproduce the tunnelling splittings observed in the H_2O and D_2O dimers [28,38] well. Recently, a hybrid potential which combines contributions of both dimer and water PESs has been reported [52]. This relies on the HBB potentials to describe the dimer interaction and the Partridge–Schwenke (PS) [55] surface for the description of the monomer behaviour.

Allowing for monomer motions within the dimer is essential for modelling dimer absorption spectra at shorter wavelengths. The question is how to do this without compromising the accuracy of the potentials discussed above, since 12D nuclear motion calculations are not feasible without further approximations. In this paper, we outline an approach that involves an effective 6D potential energy surface obtained by vibrational averaging of the 12D potential over monomer modes, which may then be used as input for 6D dimer calculations. Since we require an accurate description of the water monomers in such an approach, we combine a recent, spectroscopically determined monomer potential [56] with the HBB dimer potential to create a transferable potential energy surface that is capable of reproducing the monomer band origins to high accuracy. We check that this has no adverse effect on the dimer stationary points, and the zero point energy (ZPE) of the dimer using the diffusion Monte Carlo (DMC) method. Vibration–rotation tunnelling (VRT) levels of the H_2O and D_2O dimers are calculated using the averaging approach and compared to more standard 6D calculations which use monomers frozen in their equilibrium or their vibrational ground state geometries. These VRT states are sensitive to the quality of the PES and thus allow us to evaluate the vibrational averaging methodology employed here.

Leforestier et al. [29] developed a (6+6)*d* model that adiabatically separates the six high-frequency intramolecular modes from the six low-frequency intermolecular modes. This adiabatic approach differs from our method in the sense that they averaged the full 12D potential over the vibrational states of perturbed monomers computed at each given dimer geometry, whereas our 6D potential was obtained by averaging over the vibrational states of the free monomers. We note that the simplicity of the PES used in Ref. [29] greatly facilitated the calculation. Very recently Leforestier et al. [38] applied their adiabatic separation method to the (uncorrected) HBB potential. The calculation was kept tractable by computing the vibrational wavefunctions of the perturbed monomers for each monomer separately, so the method could be formally described as an adiabatic (3+3+6)*d* model, but they had shown in Ref. [29], that the differences with a full (6+6)*d* treatment are minimal. Detailed comparisons with the results of Leforestier et al. are given below. Similar adiabatic separation methods were applied in lower dimensionality in Refs. [53,54].

2. Method

The two water monomers in a dimer have intramolecular coordinates $\mathbf{Q}_1$ and $\mathbf{Q}_2$ which provide us with six coordinates. Additionally, the intermolecular configuration is given by geometry $\mathbf{R}$, corresponding to three Euler angles for each monomer ($\omega_1 \equiv \{\alpha_1, \beta_1, \gamma_1\}$ and $\omega_2 \equiv \{\alpha_2, \beta_2, \gamma_2\}$) and a distance R between the centre-of-mass (COM) of each monomer. However, only five Euler angles are necessary to describe the orientation of one monomer with respect to the other, therefore, in total we have 12 internal degrees of freedom (simply $3N-6$).

Any 12D water dimer (V_D^{12D}) surface can be corrected to produce a nearly exact asymptotic description of the six monomer modes using

$$V_{D+MC}^{12D}(\mathbf{Q}_1,\mathbf{Q}_2,\mathbf{R}) = V_D^{12D}(\mathbf{Q}_1,\mathbf{Q}_2,\mathbf{R}) + (V_M(\mathbf{Q}_1) + V_M(\mathbf{Q}_2) - 2V_M(\mathbf{Q}_e)) - (V_D^{12D}(\mathbf{Q}_1,\mathbf{Q}_2,\infty) - V_D^{12D}(\mathbf{Q}_e,\mathbf{Q}_e,\infty)) \quad (1)$$

where V_M is the free monomer potential function and the monomer equilibrium configuration is denoted $\mathbf{Q}_e$; the constant vector ∞ is a dimer configuration where the distance between the monomers COM's approaches infinity. Here we use a distance of $100.0a_0$ to represent the asymptote.

Here we used the HBB [28] potential as the full 12D dimer potential and the Shirin et al. (SHI08) [57] potential for the monomer contribution (V_M). The SHI08 PES is the most accurate water potential published to date: it is able to reproduce experimentally determined monomer bands up to 25,468 cm^{-1} for $J \leq 10$ with a standard deviation of only 0.1 cm^{-1} [57]. Shank et al. [52] recently corrected the HBB potential using the Partridge–Schwenke (PS) [55] monomer PES. The difference between using the PS or SHI08 monomer potential should be minimal for the energies considered here, but may become significant for higher monomer overtones the study of which is our ultimate aim.

The DVR3D software suite [58] and Radau coordinates were used to calculate vibrational wavefunctions and energies for the water monomer. Good convergence for energies up to 20 000 cm^{-1} is found with a discrete variable representation (DVR) grid based on n_r=29 radial points and $n_\theta = 40$ angular points [8,57,56]. In the DVR approximation the expectation value of an arbitrary, polynomial function f is simply given as

$$\langle \psi^i | f(\mathbf{Q}) | \psi^i \rangle = \sum w_j^i f(\mathbf{Q}_j) \tag{2}$$

where the sum runs over all DVR points and the weights, w_j, are given by the square of the amplitude of the wavefunction at the DVR point. This is important when considering the vibrational averaging approach proposed below.

The calculation of the dimer VRT levels can be performed using a rigid monomer Hamiltonian of Brocks et al. [25]

$$H = T_A + T_B + T_{AB} + V_{int} \tag{3}$$

where T_X (X is either monomer A or B), and T_{AB} correspond to the monomer and dimer kinetic energy operators, respectively, and are standard [25,32]. There are six intermolecular degrees of freedom ($\mathbf{R} = \{R, \alpha_1 - \alpha_2, \beta_1, \gamma_1, \beta_2, \gamma_2\}$), whose motions are considered variationally. The methodology is explained in some detail elsewhere [32], however, we outline some key features here.

An angular basis is employed which is constructed as a product of coupled symmetric rotor functions $D^{(j_A)}_{m_A k_A}(\boldsymbol{\omega}_1)^*$ and $D^{(j_B)}_{m_B k_B}(\boldsymbol{\omega}_2)^*$ for both the monomer rotations, where j_X corresponds to the angular momentum of monomer X, and functions $D^{(J)}_{MK}(\boldsymbol{\Omega})^*$, for the overall dimer rotation. The angular coordinates $\boldsymbol{\omega}_1$ and $\boldsymbol{\omega}_2$ define the orientations of the monomers in the dimer, and $\boldsymbol{\Omega}$ are the overall rotation angles. For H_2O, energy convergence of the dimer levels was found for a maximum j_X value of 11, whereas for the D_2O dimer the levels were converged at j_X=12 [32,28]. The PES itself is expanded in symmetric rotor functions [32,28] and the R-dependent expansion coefficients are given by

$$v_{\mathbf{\Lambda}}(R) = \frac{(2L_A+1)(2L_B+1)(2L+1)}{64\pi^4} \sum_{M_A} (-1)^{L_A+L_B+L} \times \begin{pmatrix} L_A & L_B & L \\ M_A & -M_A & 0 \end{pmatrix} \int D^{(L_A)}_{M_A K_A}(\boldsymbol{\omega}_1)^* D^{(L_B)}_{-M_A K_B}(\boldsymbol{\omega}_2)^* \times V(R, \boldsymbol{\omega}_1, \boldsymbol{\omega}_2)\, d\boldsymbol{\omega}_1\, d\boldsymbol{\omega}_2$$

where the compound index $\mathbf{\Lambda}$ runs over all values of (L_A, K_A, L_B, K_B, L) allowed by angular momentum coupling, up to some maximum value of L_A and L_B. The angular integrals in the above equation required to compute the expansion coefficients, $v_{\mathbf{\Lambda}}(R)$, are performed using L_A^{max}+1 quadrature points in each coordinate: L_A^{max}+1 point Gauss–Legendre quadrature is used for β_1 and β_2, while $2L_A^{max}$+1 point Gauss–Chebychev quadrature is used for $\alpha_1 - \alpha_2$, γ_1, and γ_2. For the Gauss–Chebychev grid, symmetry implies that only L_A^{max}+1 potential calls are actually needed. Here these quadratures were truncated at $L_A^{max} = L_B^{max}$=8, which has been shown previously to give converged eigenvalues for the full Hamiltonian [32].

For the radial basis, three contracted DVR functions create well converged low temperature spectra [32]. They were obtained on a grid containing n_R=49 equally spaced R points between 4 and 9a_0. A single, well-converged 6D dimer calculation requires the evaluation of a total of $n_R(L_A^{max} + 1)^5$ = 2 893 401 potential points.

Symmetry can be used to reduce the size of the eigenvalue problems. The water dimer has feasible quantum mechanical tunnelling paths, whereby interchange of nuclei results in equivalent minima which can be represented by the permutation-inversion (PI) group G_{16}. There are three type of these tunnelling paths (see Fig. 3, Ref. [44]): (a) acceptor tunnelling, (b) donor–acceptor interchange and (c) donor bifurcation tunnelling, which lead to splittings in the observed spectra of the water dimer. The irreducible representations of G_{16}, namely $A_1^{\pm}$, $A_2^{\pm}$, $B_1^{\pm}$, $B_2^{\pm}$ and $E^{\pm}$, are therefore used to label the water dimer VRT energy levels. Symmetry adapted basis sets for the G_{16} group are described elsewhere [32].

Three methods for dealing with monomer effects are considered: (I) with the intramolecular coordinates fixed at the equilibrium (EQ) geometry of the water monomers, (II) with these coordinates fixed at the average monomer vibrational ground state (VGS) geometry; and (III) by explicit vibrational averaging of the potential (VAP). For (III) we vibrationally average the monomer potentials at each intermolecular grid point:

$$V_{ij}^{6D}(\mathbf{R}) = \langle \psi_1^i \psi_2^j | V_{D+MC}^{12D}(\mathbf{Q}_1, \mathbf{Q}_2; \mathbf{R}) | \psi_1^i \psi_2^j \rangle \tag{4}$$

where ψ_n are the monomer wavefunctions of monomers 1 and 2, in vibrational states i and j, respectively. When averaging the monomer corrected potential, the problem can be split into several averages and constants:

$$\begin{aligned} &\langle \psi_1^i \psi_2^j | V_{D+MC}^{12D}(\mathbf{Q}_1, \mathbf{Q}_2; \mathbf{R}) | \psi_1^i \psi_2^j \rangle \\ &\quad = \langle \psi_1^i \psi_2^j | V_D^{12D}(\mathbf{Q}_1, \mathbf{Q}_2; \mathbf{R}) | \psi_1^i \psi_2^j \rangle \\ &\qquad + [\langle \psi_1^i | V_M(\mathbf{Q}_1) | \psi_1^i \rangle + \langle \psi_2^j | V_M(\mathbf{Q}_2) | \psi_2^j \rangle \\ &\qquad - 2V_M(\mathbf{Q}_e)] - [\langle \psi_1^i | V_D^{12D}(\mathbf{Q}_1, \mathbf{Q}_e, \infty) | \psi_1^i \rangle \\ &\qquad + \langle \psi_2^j | V_D^{12D}(\mathbf{Q}_e, \mathbf{Q}_2, \infty) | \psi_2^j \rangle - 2V_D^{12D}(\mathbf{Q}_e, \mathbf{Q}_e, \infty)] \end{aligned} \tag{5}$$

which reduces the computational cost by avoiding unnecessary averaging over the full potential. Additionally, since the input for the 6D calculations is the interaction energy, V_{int}, several constants cancel, leaving

$$\begin{aligned} V_{int}^{ij} = &\langle \psi_1^i \psi_2^j | V_D^{12D}(\mathbf{Q}_1, \mathbf{Q}_2; \mathbf{R}) | \psi_1^i \psi_2^j \rangle \\ &- [\langle \psi_1^i | V_D^{12D}(\mathbf{Q}_1, \mathbf{Q}_e, \infty) | \psi_1^i \rangle \\ &+ \langle \psi_2^j | V_D^{12D}(\mathbf{Q}_e, \mathbf{Q}_2, \infty) | \psi_2^j \rangle - V_D^{12D}(\mathbf{Q}_e, \mathbf{Q}_e, \infty)] \end{aligned} \tag{6}$$

so that all monomer corrections are removed. However, the monomer PES still contributes since the monomer wavefunctions depend on it.

The monomer wavefunctions (ψ_n) can either take the form of: (I) a single set of monomer wavefunctions for the whole averaging procedure, as in this work, or (II) perturbed monomer wavefunctions computed at each intermolecular grid point, as in the work of Leforestier et al. [38]. Since a typical intermolecular grid is around 3×10^6 points, the latter approach would be significantly more expensive if the perturbed wavefunctions of both

monomers were computed simultaneously. In Ref. [38] they were obtained for each monomer separately, while the other monomer was frozen at its equilibrium geometry for a given intermolecular grid point. Both approaches require a good variational method (such as DVR3D) for calculating the monomer wavefunctions.

Here we average the potential over the wavefunctions of the free monomers at each intermolecular grid point. This in itself is a computationally demanding task since we now have $[n_\theta n_r(n_r+1)/2]^2 \times n_R(L_A^{\max}+1)^5$ unique grid points and associated potential calls. For the DVR3D calculations we used a small basis, $(n_r, n_\theta) = (7, 24)$ [59], which converges band origins up to 12 000 cm^{-1}. These parameters lead to 1 306 613 597 184 potential calls which would take around 7000 days on a single CPU to compute. However, the averages at each point on the dimer grid are completely independent from one another: an ideal case for grid computing.

Furthermore, storing this number of PES points would occupy about 10 TB of disk or memory, so that the averaging must be done on the fly. Our program calculates and stores the potentials points required for each dimer point 6D average, the average is calculated for each required monomer vibrational state *ij* and the original potential points are discarded. This procedure is repeated for each dimer grid point. This algorithm means that many effective potential *ij* monomer vibrational state averages can be computed at once at no significant additional computational cost.

We performed our potential averaging calculations on the University College London (UCL) Research Computing Condor grid facility [60] which uses the Condor grid software [61] developed at the University of Wisconsin. The facility itself has a pool of up to 1400 Windows PCs, each with varying clock-speeds (between 1 and 3 GHz) and between 256 MB and 1 GB RAM. The grid harnesses unused PCs from the UCL windows terminal service (WTS) cluster network. The calculations for the dimer grid with wavefunctions defined on {7, 7, 24} DVR grids took around 2 weeks to complete.

3. Results

3.1. Ground state properties of the water potential

In Table 1 we give some characteristics of the equilibrium of the monomer. It can be seen that in comparison to the benchmark monomer potential, the uncorrected HBB dimer potential gives slightly larger O–H bond lengths and a bond angle smaller by about 0.3°. The geometry of the barrier to linearity is also reproduced fairly well. However, the energy of the barrier is not so well represented, unless the monomer correction is made. It should be noted that a potential which produces an accurate change from the equilibrium to the linear geometry is a good starting point for accurate calculations of vibrational band origins [62]. By adding the monomer correction, we end up with the monomer characteristics of the SHI08 potential.

However, the correction of the potential will shift the stationary points on the water dimer surface. To investigate the size of the changes, we re-evaluated the stationary points on the modified dimer surface and the results are given in Table 2, as well as the previous HBB and the benchmark results by Tschumper et al. [63]. As can be seen, the difference between the HBB and monomer-corrected potentials is minimal. The agreement of all the potentials in the table with the benchmark results is found to be good.

3.2. Water monomer energy levels

To study the water monomer eigen-problem using a dimer potential surface we fix one molecule in the free monomer equilibrium geometry and put it at a distance of $R = 100a_0$. The corresponding absolute error for each set of vibrational band origins with respect to experimentally determined values [64] is shown in Fig. 1 up to 16 000 cm^{-1}.

Table 2
Energies of the 10 stationary points found on the modified 12D water dimer surface (columns 5 and 6).

Structure	Symmetry	Energies (cm^{-1})		
		HBB [28]	HBB+SHI08	Benchmark [63]
1	C_s	0.0	0.0	0
2	C_1	161.4	159.6	181
3	C_s	198.5	193.5	198
4	C_i	244.0	241.1	245
5	C_2	329.3	323.9	323
6	C_{2h}	348.1	340.6	348
7	C_s	603.0	601.3	635
8	C_{2h}	1181.8	1178.9	1249
9	C_{2v}	590.2	588.2	625
10	C_{2v}	898.3	894.8	948

Note that these energies are relative to the water dimer equilibrium geometry (stationary point 1). All energies are given in cm^{-1}.

Table 1
Monomer equilibrium characteristics.

PES name	PES type	r_{eq} (å)	$\angle HOH_{eq}$ (deg)	r^{vgs} (å)	$\angle HOH_{vgs}$ (deg)	r_{linear} (å)	Barrier (cm^{-1})
HBB [28]	H_2O dimer	0.96151	104.22	0.98687	104.09	0.93768	11 205.6
SHI08 [56]	H_2O monomer	0.95785	104.51	0.97565	104.43	0.93327	11 120.1
HBB [28]	D_2O dimer			0.98193	104.09		
SHI08 [56]	D_2O monomer			0.97078	104.42		
Experiment		0.95785 [73]	104.50 [73]				11114 ± 5 [74]

The equilibrium geometry for H_2O and D_2O are the same and are given by the bond length r_{eq} and the bond angle, $\angle HOH_{eq}$. The average vibrational ground state geometry is given by the bond length r_{vgs} and the bond angle, $\angle HOH_{vgs}$. The bond length for linear HOH is given by r_{linear}.

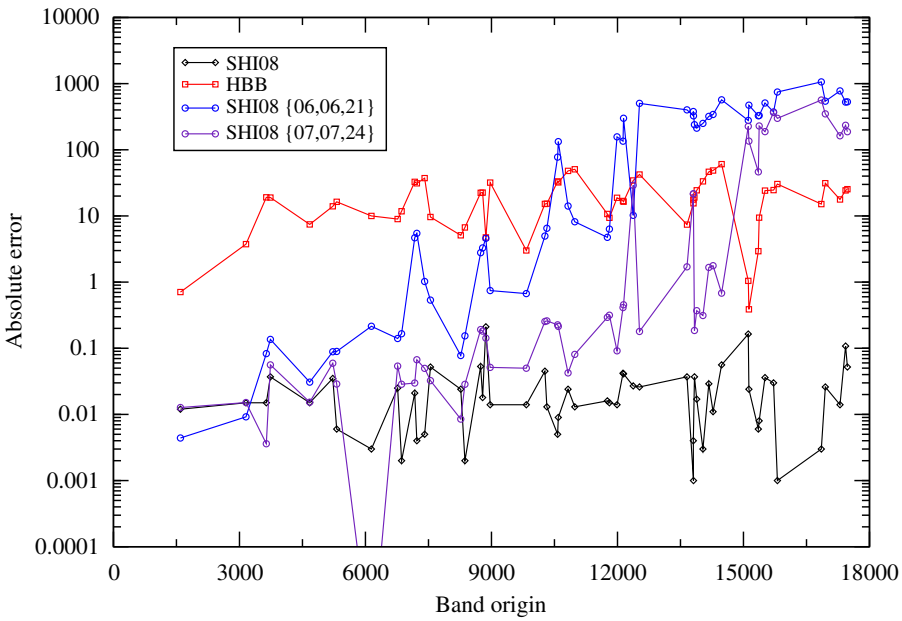

Fig. 1. Absolute error in the calculated band origins of water with respect to experimental values [64] for different potentials and basis sets. The errors are plotted on a logarithmic scale in cm^{-1}.

It can be seen that the agreement between the SHI08 band origins [56] and the experimental values are extremely good. In comparison, the monomer band origins for the HBB potential are not as good, and they become rapidly worse for higher bands.

Since we are interested in the large averaging calculations, we also show results for two significantly reduced monomer basis sets in Fig. 1, for (n_r, n_θ) equal to (6,21) and (7,24) DVR points, respectively. The Morse parameters in these DVR3D calculations were optimized for small basis sets [59]. For each n_r, we converged the number of accurate band origins for increasing n_θ. Good values of n_θ are found to be 21 and 24, for n_r equal to 6 and 7, respectively; the angular grid needs to be larger than the radial one as water has two bending states for every stretching state.

It can be seen that the smaller basis $\{6,6,21\}$ only gives relatively good accuracy up to around 4000 cm^{-1} whereas the $\{7,7,24\}$ basis performs relatively well up to about 12 000 cm^{-1}.

The zero-point energy for water with the SHI08 potential (and the large basis set) was found to be 4638.1 cm^{-1}, in comparison with the HBB value of 4615.9 cm^{-1}. These differences are important when considering the dimer ZPE below.

3.3. Water dimer vibration–rotation–tunnelling level spectra

First of all, in this section, we discuss the DMC simulations to calculate D_0 for the corrected water dimer potential (HBB+SHI08). Following procedures outlined by Bowman and co-workers [28,51,65,66] we solve the Schrodinger equation in imaginary time with the diffusion Monte Carlo (DMC) method [67–70].

Table 3
D_0 and D_e values for the various calculations including calculations with monomers fixed in their equilibrium (EQ) and vibrational ground state (VGS) geometries, as well as calculations with a vibrationally averaged potential (VAP).

Dimer	Method	Potential	D_0 value (cm^{-1})	D_e value (cm^{-1})
$(H_2O)_2$	12D	HBB		1665.8
	12D	HBB+SHI08		1657.1
	EQ geometry	HBB	998.0	1656.8
		HBB+SHI08	993.0	1648.3
	VGS geometry	HBB	1029.9	1709.4
		HBB+SHI08	1025.1	1700.9
	VAP	HBB/SHI08	1005.1	1683.3
	(6+6)*d* [38]	HBB/HBB	1021.7	
	12D DMC [28]	HBB	1040	
	12D DMC	HBB+SHI08	1034	
$(D_2O)_2$	12D	HBB		1665.8
	12D	HBB+SHI08		1657.1
	EQ geometry	HBB	1137.8	1656.8
		HBB+SHI08	1120.8	1648.3
	VGS geometry	HBB	1172.6	1694.4
		HBB+SHI08	1158.3	1686.0
	VAP	HBB/SHI08	1142.3	1671.5
	(6+6)*d* [38]	HBB/HBB	1161.0	
	12D DMC [28]	HBB	1169	
	12D DMC	HBB+SHI08	1168	

Potentials with a slash indicate an averaging technique where the potential is averaged over the first with monomer wavefunctions calculated from the second.

We performed 10 calculations for the HBB+SHI08 potential, each with a sample size of 20 000 replicas. Each replica takes a random walk in 12D Cartesian space and at each time step can be kept alive, destroyed, or replicated depending on a probability deduced on a reference energy at each imaginary time step ($d\tau$). The calculations were

Table 4
H_2O VRT levels, tunnelling splittings, and rotational constants (in cm^{-1}).

K	PES		o_1	o_2	a	i_1	i_2	$B+C$	A
Ground state (A')									
0	EQ geometry	HBB	0.00	13.30	13.30	0.742	0.639	0.4112	
		HBB+SHI08	0.00	13.63	13.63	0.747	0.639	0.4114	
	VGS geometry	HBB	0.00	12.19	12.19	0.781	0.678	0.4119	
		HBB+SHI08	0.00	12.57	12.57	0.789	0.679	0.4121	
	VAP	HBB/SHI08	0.00	11.90	11.90	0.798	0.700	0.4126	
	(6+6)*d* [38]	HBB/HBB	0.00	10.83	10.83	0.717	0.647	0.3998	
	Exp		0.00	11.18[a]		0.752	0.651	0.4112	
1	EQ geometry	HBB	15.72	12.51	3.21	0.689	0.517	0.4111	7.47
		HBB+SHI08	15.90	12.59	3.31	0.692	0.520	0.4113	7.43
	VGS geometry	HBB	15.11	12.19	2.93	0.736	0.548	0.4118	7.55
		HBB+SHI08	15.32	12.28	3.04	0.741	0.553	0.4120	7.52
	VAP	HBB/SHI08	15.04	12.12	2.92	0.749	0.571	0.4125	7.63
	(6+6)*d* [38]	HBB/HBB	14.33	11.95	2.37	0.677	0.522		7.73
	Exp		14.39	11.66		0.705	0.541	0.4108	7.44/7.59
Donor torsion (A'')									
0	EQ geometry	HBB	116.12	60.85	55.27	6.340	2.369	0.4138	
		HBB	116.09	60.24	55.84	6.395	2.412	0.4141	
	VGS geometry	HBB	115.64	62.53	53.11	6.177	2.480	0.4143	
		HBB+SHI08	115.58	61.75	53.83	6.330	2.548	0.4147	
	VAP	HBB/SHI08	115.59	64.00	51.59	6.930	2.654	0.4152	
	(6+6)*d* [38]	HBB/HBB	116.03	66.15	49.88				
	Exp		116[b]	64.52			2.540		
1	EQ geometry	HBB	85.93	92.72	6.79	1.024	3.300	0.4124	0.84
		HBB+SHI08	85.56	92.62	7.06	1.111	3.370	0.4127	0.92
	VGS geometry	HBB	86.66	92.57	5.91	0.890	3.361	0.4127	0.53
		HBB+SHI08	86.19	92.36	6.17	1.001	3.463	0.4131	0.61
	VAP	HBB/SHI08	87.95	93.66	5.71	1.104	3.590	0.4135	1.01
	(6+6)*d* [38]	HBB/HBB	89.52	93.49	3.97				
	Exp		87.75			1.110		0.4083	
Acceptor wag (A')									
0	EQ geometry	HBB	106.97	106.10	0.88	3.880	0.006	0.4109	
		HBB+SHI08	107.25	106.28	0.96	4.181	0.012	0.4112	
	VGS geometry	HBB	105.98	106.07	0.09	3.418	0.031	0.4115	
		HBB+SHI08	106.27	106.18	0.09	3.418	0.031	0.4115	
	VAP	HBB/SHI08	106.02	105.85	0.16	3.368	0.087	0.4119	
	(6+6)*d* [38]	HBB/HBB	103.52	103.26	0.26				
	Exp		107.93	108.89	0.96	2.951	0.017	0.4094	
1	EQ geometry	HBB	106.87	121.25	14.38	5.498	3.498	0.4122	7.52
		HBB+SHI08	106.87	121.27	14.40	5.555	3.645	0.4125	7.30
	VGS geometry	HBB	107.42	121.34	13.92	5.596	3.536	0.427	8.35
		HBB+SHI08	107.33	121.29	13.96	5.659	3.708	0.4130	8.08
	VAP	HBB/SHI08	107.20	121.14	13.94	5.561	3.699	0.4133	8.24
	(6+6)*d* [38]	HBB/HBB	106.19	119.79	13.60				
	Exp		109.98	123.56	13.58	5.238	3.412	0.4122	8.08
Acceptor twist (A'')									
0	EQ geometry	HBB	130.27	116.33	13.94	1.104	9.623	0.4117	
		HBB+SHI08	130.84	116.20	14.64	1.230	9.796	0.4119	
	VGS geometry	HBB	128.95	117.53	11.43	0.327	9.826	0.4123	
		HBB+SHI08	129.55	117.40	12.15	0.559	10.053	0.4126	
	VAP	HBB/SHI08	130.35	117.63	12.72	0.885	9.837	0.4127	
	(6+6)*d* [38]	HBB/HBB	128.29	118.60	9.69				
	Exp			120.19				0.4138	
1	EQ geometry	HBB	141.28	135.16	6.12	4.266	5.641	0.4115	14.92
		HBB+SHI08	141.70	135.44	6.05	4.297	5.688	0.4117	14.95
	VGS geometry	HBB	141.40	135.49	5.91	4.608	5.832	0.4121	15.21
		HBB+SHI08	141.88	135.89	5.79	4.668	5.886	0.4123	15.30
	VAP	HBB/SHI08	141.15	135.68	5.48	4.820	5.799	0.4126	14.42
	(6+6)*d* [38]	HBB/HBB	140.19	134.39	5.80				
Donor torsion overtone (A')									
0	EQ geometry	HBB	127.16	147.75	20.58	8.886	1.267	0.4077	
		HBB+SHI08	126.67	147.73	21.06	8.858	1.275	0.4078	

Table 4 (*continued*)

K	PES		o_1	o_2	a	i_1	i_2	$B+C$	A
	VGS geometry	HBB	128.47	148.91	20.43	9.847	1.439	0.4089	
		HBB+SHI08	127.72	148.97	21.24	10.005	1.467	0.4092	
	VAP	HBB/SHI08	129.07	147.79	18.72	9.537	1.426	0.4093	
	(6+6)*d* [38]	HBB/HBB	130.46	145.83	15.37				
	Exp			153.62			1.877		
1	EQ geometry	HBB	149.86	147.09	2.77	1.431	1.657	0.4033	11.02
		HBB+SHI08	149.61	146.79	2.82	1.488	1.680	0.4035	11.00
	VGS geometry	HBB	151.72	149.20	2.52	1.532	1.869	0.4047	11.77
		HBB+SHI08	151.48	148.86	2.62	1.640	1.983	0.4050	11.82
	VAP	HBB/SHI08	150.93	148.68	2.25	1.498	1.566	0.4050	11.37
	(6+6)*d* [38]	HBB/HBB	149.51	147.49	2.02				
Stretch (*A*′)									
0	EQ geometry	HBB	140.14	183.82	43.69	2.717	19.131	0.4089	
		HBB+SHI08	139.80	183.88	44.08	2.739	19.309	0.4091	
	VGS geometry	HBB	142.97	183.83	40.86	2.755	18.741	0.4093	
		HBB+SHI08	142.62	183.94	41.31	2.751	19.120	0.4095	
	VAP	HBB/SHI08	142.44	183.46	41.02	3.368	19.851	0.4104	
	(6+6)*d* [38]	HBB/HBB	141.78	182.30	40.52				

Results for four variations of the HBB potential are given: (1) simply the HBB potential [28] with monomers in EQ geometry; (2) HBB+SHI08 (monomer correction of SHI08 potential) again with monomers in the EQ geometry; (3) HBB with monomers in the VGS geometry; (4) HBB+SHI08 with monomers in the VGS geometry. Experimental data are also given, where available [40,41,45,30,31]. Assignment of the intermolecular vibrations is outlined in Ref. [33]. Potentials with a slash indicate an averaging technique where the potential is averaged over the first with monomer wavefunctions calculated from the second.

[a] Note that the experimental GS acceptor splitting is estimated to be 11.18 cm^{-1} (see Ref. [32]).

[b] Result measured in Neon Matrix [75,76].

Table 5
D_2O VRT levels, tunnelling splittings, and rotational constants (in cm^{-1}).

K	PES		o_1	o_2	a	i_1	i_2	$B+C$	A
Ground state (*A*′)									
0	EQ	HBB	0.00	2.36	2.36	0.040	0.036	0.3708	
		HBB+SHI08	0.00	2.49	2.49	0.040	0.036	0.3708	
	VGS	HBB	0.00	2.05	2.05	0.041	0.038	0.3714	
		HBB+SHI08	0.00	2.18	2.18	0.042	0.039	0.3715	
	VAP	HBB/SHI08	0.00	2.01	2.01	0.043	0.040	0.3719	
	(6+6)*d* [38]		0.00	1.74	1.74	0.039	0.036	0.3547	
	Exp		0.00	1.71	1.71	0.039	0.036	0.3622	
1	EQ	HBB	5.75	4.99	0.76	0.036	0.033	0.3708	4.19
		HBB+SHI08	5.84	5.04	0.80	0.036	0.033	0.3708	4.20
	VGS	HBB	5.52	4.87	0.65	0.038	0.035	0.3714	4.18
		HBB+SHI08	5.62	4.93	0.70	0.039	0.035	0.3715	4.19
	VAP	HBB/SHI08	5.52	4.87	0.65	0.040	0.036	0.3719	4.19
	(6+6)*d* [38]	HBB/HBB	5.29	4.77	0.52	0.036	0.033		4.16
	Exp		5.36	4.74	0.62	0.036	0.033	0.3621	4.17
Donor torsion (*A*″)									
0	EQ	HBB	75.62	55.97	19.65	0.299	0.173	0.3700	
		HBB+SHI08	75.38	55.13	20.26	0.311	0.177	0.3701	
	VGS	HBB	75.84	57.97	17.86	0.289	0.182	0.3705	
		HBB+SHI08	75.54	57.00	18.54	0.307	0.189	0.3707	
	VAP	HBB/SHI08	76.42	58.84	17.58	0.356	0.204	0.3712	
	(6+6)*d* [38]		76.67	60.50	16.17				
	Exp		75.38	59.59	15.81	0.328	0.203	0.3622	
1	EQ	HBB	65.30	69.60	4.30	0.093	0.221	0.3691	1.66
		HBB+SHI08	64.59	69.05	4.46	0.099	0.226	0.3692	1.57
	VGS	HBB	66.92	70.83	3.91	0.095	0.232	0.3696	1.97
		HBB+SHI08	66.11	70.18	4.06	0.102	0.240	0.3698	1.87
	VAP	HBB/SHI08	67.80	71.58	3.78	0.117	0.265	0.3702	2.06
	(6+6)*d* [38]	HBB/HBB	69.20	72.21	3.01				
	Exp		68.27	71.81	3.54	0.132	0.257	0.3600	2.56
Acceptor wag (*A*′)									
0	EQ	HBB	78.96	80.39	1.43	0.145	0.110	0.3698	
		HBB+SHI08	78.76	80.16	1.40	0.145	0.110	0.3699	
	VGS	HBB	79.84	81.54	1.70	0.146	0.114	0.3700	
		HBB+SHI08	79.51	81.19	1.68	0.147	0.115	0.3702	

Table 5 (*continued*)

K	PES		o_1	o_2	a	i_1	i_2	$B+C$	A
	VAP	HBB/SHI08	79.96	81.43	1.46	0.163	0.128	0.3706	
	(6+6)*d* [38]	HBB/HBB	78.82	80.15	1.33				
	Exp		82.64	84.40	1.77	0.131	0.112	0.3603	
1	EQ	HBB	81.97	86.23	4.26	0.418	0.180	0.3705	4.42
		HBB+SHI08	81.72	86.11	4.39	0.422	0.185	0.3706	4.45
	VGS	HBB	83.13	87.02	3.89	0.433	0.180	0.3708	4.39
		HBB+SHI08	82.79	86.82	4.04	0.437	0.185	0.3709	4.46
	VAP	HBB/SHI08	82.98	87.06	4.09	0.446	0.193	0.3713	4.32
	(6+6)*d* [38]	HBB/HBB	82.13	85.73	3.60				
	Exp		85.57	89.56	4.00	0.398	0.168	0.3592	4.05
Acceptor twist (*A″*)									
0	EQ	HBB	90.28	87.53	2.75	0.460	0.841	0.3717	
		HBB+SHI08	90.46	87.46	3.00	0.448	0.861	0.3717	
	VGS	HBB	90.60	88.32	2.28	0.524	0.864	0.3723	
		HBB+SHI08	90.80	88.26	2.54	0.511	0.887	0.3723	
	VAP	HBB/SHI08	90.94	88.32	2.62	0.499	0.890	0.3726	
	(6+6)*d* [38]	HBB/HBB	90.28	88.39	1.89				
	Exp		92.91	90.37	2.54	0.432	0.443	0.3665	
1	EQ	HBB	96.15	93.79	2.36	0.500	0.648	0.3718	6.06
		HBB+SHI08	96.17	93.82	2.35	0.509	0.655	0.3718	6.04
	VGS	HBB	96.71	94.37	2.35	0.523	0.684	0.3724	6.08
		HBB+SHI08	96.74	94.41	2.33	0.536	0.693	0.3724	6.05
	VAP	HBB/SHI08	96.73	94.44	2.29	0.549	0.696	0.3727	5.95
	(6+6)*d* [38]	HBB/HBB	96.15	94.12	2.03				
Donor torsion overtone (*A′*)									
0	EQ	HBB	98.81	129.95	31.14	0.750	1.142	0.3686	
		HBB+SHI08	97.88	129.78	31.89	0.786	1.220	0.3688	
	VGS	HBB+SHI08	101.28	130.58	29.30	0.759	1.056	0.3691	
		HBB+SHI08	100.19	130.40	30.20	0.807	1.160	0.3694	
	VAP	HBB/SHI08	102.12	130.61	28.50	0.828	1.221	0.3696	
	(6+6)*d* [38]	HBB/HBB	103.74	130.02	26.28				
	Exp		104.24			0.783		0.3632	
1	EQ	HBB	122.82	114.47	8.35	0.444	0.029	0.3700	4.27
		HBB+SHI08	122.61	114.08	8.53	0.486	0.024	0.3703	4.51
	VGS	HBB	123.22	115.45	7.77	0.411	0.036	0.3702	3.40
		HBB+SHI08	122.85	114.89	7.96	0.452	0.031	0.3705	3.58
	VAP	HBB/SHI08	124.54	116.70	7.84	0.492	0.021	0.3708	4.25
	(6+6)*d* [38]	HBB/HBB	124.27	117.39	6.88				
Donor torsion+acceptor wag combination (*A″*)									
0	EQ	HBB	129.37	136.14	6.77	0.002	1.148	0.3703	
		HBB+SHI08	128.65	135.95	7.30	0.009	1.311	0.3705	
	VGS	HBB	131.58	136.48	4.91	0.031	0.863	0.3703	
		HBB+SHI08	130.64	136.18	5.54	0.019	0.991	0.3706	
	VAP	HBB/SHI08	132.04	137.46	5.42	0.014	1.040	0.3709	
	(6+6)*d* [38]	HBB/HBB	132.60	136.91	4.31				
Stretch (*A′*)									
	EQ	HBB	131.37	141.78	10.41	1.954	2.148	0.3680	
		HBB+SHI08	130.68	141.55	10.87	2.128	2.188	0.3682	
	VGS	HBB	133.65	142.71	9.07	1.867	2.169	0.3694	
		HBB+SHI08	132.90	142.41	9.51	2.107	2.219	0.3697	
	VAP	HBB/SHI08	133.17	142.65	9.48	1.771	2.345	0.3689	
	(6+6)*d* [38]	HBB/HBB	133.50	142.73	9.23				

Results for four variations of the HBB potential are given: (1) simply the HBB potential [28] with monomers in EQ geometry; (2) HBB+SHI08 (monomer correction of SHI08 potential) again with monomers in the EQ geometry; (3) HBB with monomers in the VGS geometry; (4) HBB+SHI08 with monomers in the VGS geometry. Experimental data are also given, where available [40,41,45,30,31]. Assignment of the intermolecular vibrations is outlined in Ref. [33]. Potentials with a slash indicate an averaging technique where the potential is averaged over the first with monomer wavefunctions calculated from the second.

run for 4000 steps with a large time step (25 au) to allow for quick equilibration of the system, followed by 6000 steps with a smaller time step (5 au), which allows for good convergence in the zero-point energy of the dimer. One important feature of a DMC calculation is the feedback parameter, α which is used [69,70]. As a general rule it is a good idea to start by using a value around $1/d\tau$ and then see which value keeps the population approximately constant. In our simulations, we choose α to be 0.03 or 0.09 dependent on whether we were in the equilibration, or the convergence stage of the calculation.

The zero-point energy of the H_2O dimer with the HBB+SHI08 potential was found to be $9899 \pm 5\,cm^{-1}$ with the DMC method. DMC is a statistical method and $\pm 5\,cm^{-1}$ is the error estimate. The difference between these results and the original HBB DMC result for the

water dimer ($9854 \pm 3\,cm^{-1}$) can be explained by the differences in the monomer zero-point energies ($23\,cm^{-1}$ for each monomer). The ZPE for the D_2O dimer using DMC was found to be $7272 \pm 5\,cm^{-1}$.

In comparison, the dissociation energies, D_e and D_0, for $(H_2O)_2$ and $(D_2O)_2$ are given for the various calculations in Table 3. There is a lowering of $8.7\,cm^{-1}$ in D_e in the monomer corrected potential (HBB+SHI08) with respect to the original (HBB) dimer potential. Nearly the same lowering of D_e was found in the 6D potentials with the monomers frozen either at their equilibrium geometry or at their vibrationally averaged geometry. The corresponding lowering of D_0 is about $5\,cm^{-1}$ for $(H_2O)_2$, but much larger for $(D_2O)_2$, which shows that effects other than just the well depth also play a role. The reduction of D_e by freezing the monomers at their equilibrium geometry is about $9\,cm^{-1}$, for both the HBB potential and the HBB+SHI08 potential.

As it was already observed by Leforestier et al. [38], the values of D_e and D_0 obtained from the HBB potential become considerably larger when the monomers are fixed at their vibrationally averaged (VGS) geometry, rather than at their equilibrium (EQ) geometry. It was explained that this is due to the fact that the values of D_e for the 6D intermolecular potentials with frozen monomers are given relative to the energies of the free monomers at the same geometries. Obviously, the monomer energy is much higher at the VGS geometry than at the EQ geometry. It is also clear why the differences are smaller for $(D_2O)_2$ than for $(H_2O)_2$; the VGS geometry of D_2O differs less from the EQ geometry than it does for H_2O. The

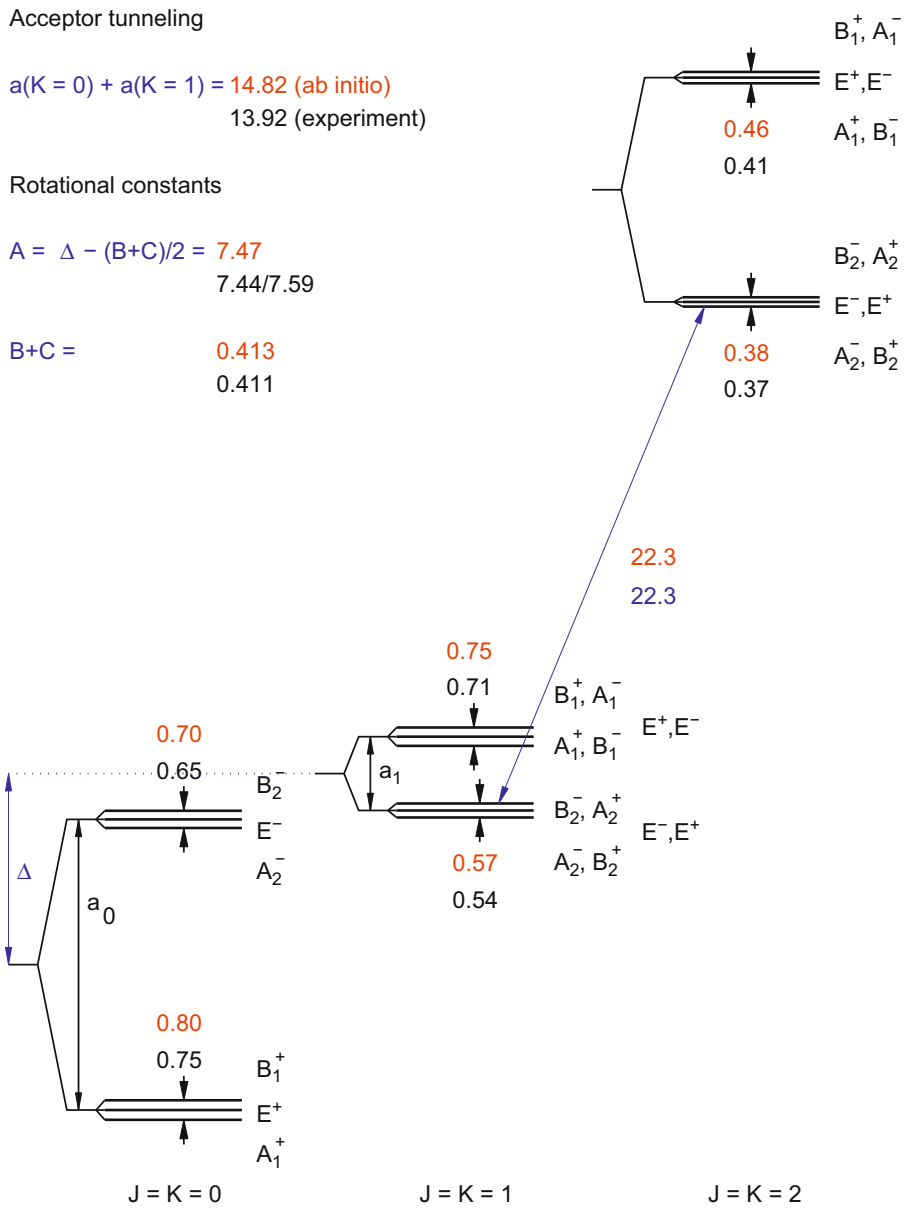

Fig. 2. Ground state H_2O VRT levels (cm^{-1}) from converged calculations of the HBB+SHI08 potential with the vibrational averaging technique (upper numbers, in red) in comparison with experimental data [40,41,45,30,31] (lower numbers). (For interpretation of the references to colour in this figure legend, the reader is referred to the web version of this article.)

corresponding differences for the HBB+SHI08 potential are similar to those found for the original HBB potential.

The value of D_e for the vibrationally averaged potential (VAP) was defined relative to the energy of the free monomers in their vibrational ground state. It was calculated by subtracting the value of the VAP potential at the minimum from its value for two monomers at a distance of $100a_0$. These values of D_e and the corresponding values of D_0 are somewhat larger than the values for the monomers frozen at their EQ geometries. Obviously, and this is a feature commonly observed in noncovalent interactions, the interaction between vibrating monomers is stronger than between rigid monomers at their EQ geometry. The effect is larger for $(H_2O)_2$ than for $(D_2O)_2$ because of the larger amplitude of the monomer vibrations. The "artificial" increase of D_e due to the higher energy of the monomers at their VGS geometries does not occur when the monomers are truly vibrating.

The differences between our D_0 values from the VAP potential and the values reported from the (6+6)*d* method [38] shown in Table 3 can be understood from the fact that the 6D VAP was obtained by averaging the 12D potential over the vibrational ground state of the free monomers, whereas the adiabatic 6D potential in the (6+6)*d* method corresponds to averaging the 12D potential over the interacting monomers in the dimer. These interactions lead to shifts of the monomer fundamental frequencies. The dominant shift is a large red shift (about $50\,cm^{-1}$) of the stretch frequency of the donor OH group directly involved in the hydrogen bond; the frequency shifts of all other intramolecular modes are much smaller. It may therefore be expected that also the intramolecular zero-point energy is lowered in the dimer with respect to the free monomers. This effect is included in the (6+6)*d* method, but not in the VAP results. Hence, one may expect that the total vibrational zero-point energy is smaller in (6+6)*d* than in VAP, and that D_0 is larger for (6+6)*d* than for VAP.

The D_0 values may also be compared with the full 12D DMC calculations, which for the HBB+SHI08 (HBB [28])

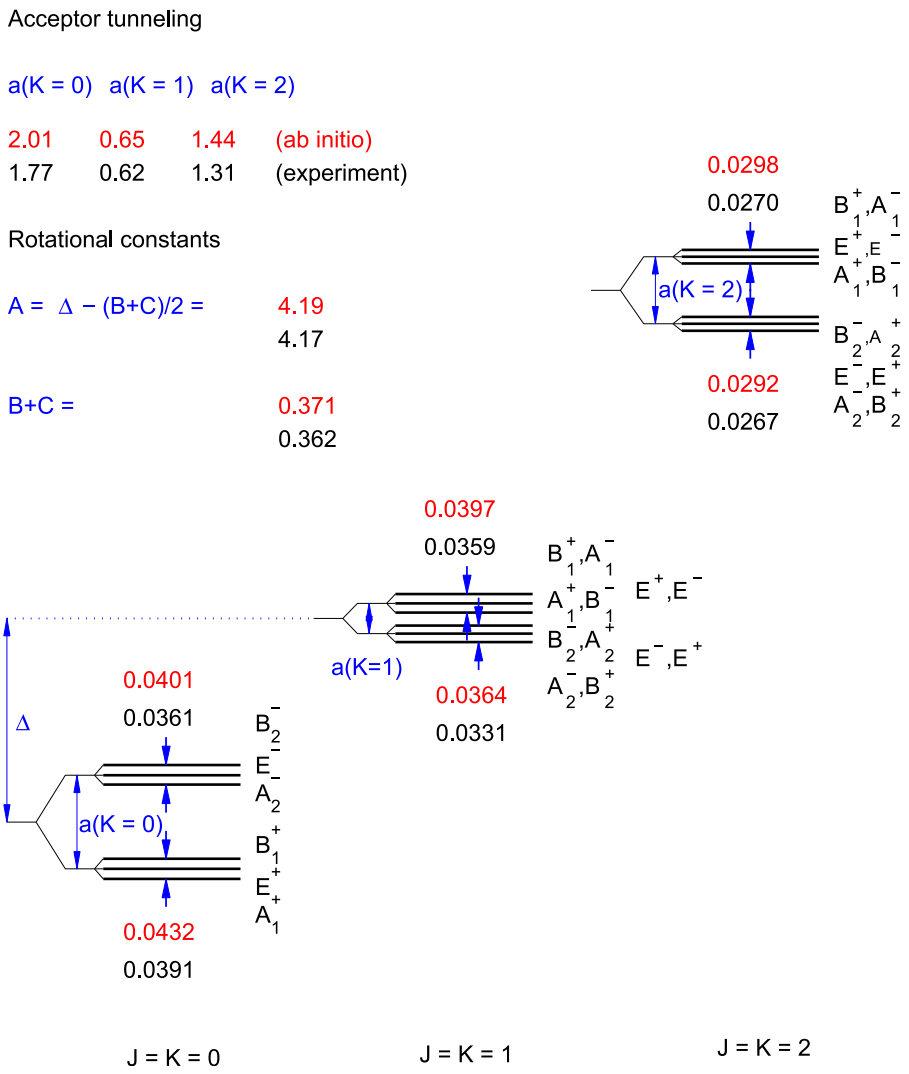

Fig. 3. Ground state D_2O VRT levels (cm^{-1}) from converged calculations of the HBB+SHI08 potential (upper numbers, in red) in comparison with experimental data [40,41,45] (lower numbers). (For interpretation of the references to colour in this figure legend, the reader is referred to the web version of this article.)

potential are 1034 cm^{-1} (1040 cm^{-1}) for $(H_2O)_2$, and 1168 cm^{-1} (1169 cm^{-1}) for $(D_2O)_2$, see Table 3. The fact that the vibrationally averaged geometry (VGS) results are closest to the DMC results is purely accidental; it is caused by the "artificial" increase of D_e in the VGS method explained above. The fact that, otherwise, the values of D_0 obtained from the (6+6)*d* method are closest to the DMC values obtained from the full 12D potential should be clear from the explanations above. It should also be remembered, of course, that the DMC method is an approximate numerical method and our errors are estimated to be $\pm 5\ cm^{-1}$.

The properties of the VRT states with K=0 and 1 calculated with the HBB potentials are listed and compared with the available experimental data in Tables 4 and 5 for the H_2O and D_2O dimers, respectively. Note that the origins o_1 and o_2 for K=1 are not simply the energy levels calculated for J=1; the quantity $(B+C)/2$ is subtracted.

We present VRT states for the HBB and the modified HBB+SHI08 potential for three types of calculations: (1) monomers in their equilibrium (EQ) geometries, (2) monomers in their vibrationally averaged ground state (VGS) geometries (which are taken as the expected geometries from the DVR3D wavefunctions), and (3) vibrationally averaged potential (VAP). Tables 4 and 5 compare our results with the (6+6)*d* calculations of Leforestier et al. [38]. These workers also computed EQ and VGS results; at low energies these results are in close agreement. At higher energies the results of Leforestier et al. become slightly lower than ours with the largest difference being 1 cm^{-1} in o_1 of the K=1 donor torsion overtone. These differences can be accounted for by differences in the nuclear motion treatments. Leforestier et al. used a potential-optimized DVR scheme for the radial coordinate, starting from a sine basis, while we used contracted sinc DVR radial basis functions. Perhaps more significantly, Leforestier et al. evaluated the matrix

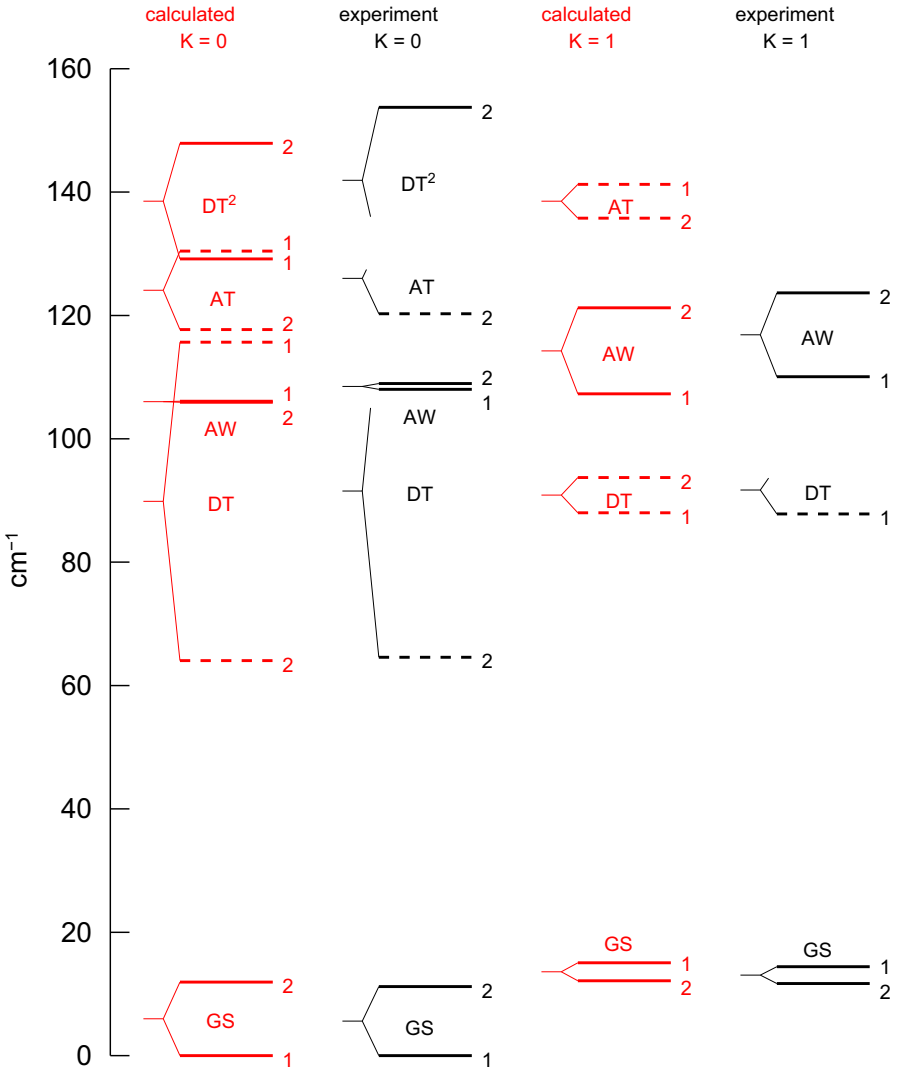

Fig. 4. VRT levels of the H_2O dimer corresponding to the intermolecular vibrations, calculated from the HBB+SHI08 potential and the vibrational averaging methodology, in comparison with experimental data [45]. The levels 1 and 2 are the origins, o_1 and o_1, of the A_1, E_1, B_1 and A_2, E_2, B_2 levels, respectively. The abbreviations GS, DT, AW, and AT denote the ground state (A'), donor torsion (A''), acceptor wag (A'), and acceptor twist (A'') modes [45,34]. Solid lines refer to A' symmetry, dashed lines to A'' symmetry, with respect to the point group C_s of the equilibrium structure. Note that those experimental levels which are not given have not been measured to date.

elements of the potential over the angular basis functions by numerical quadrature, whereas we used a spherical expansion of the potential (truncated at $L_A^{max}=8$), and computed the angular integrals analytically. Finally, we neglect the off-diagonal Coriolis coupling, making K an exact quantum number, while Leforestier et al. include these terms. The latter affects mainly the rotational constants. However, it was recently shown that the differences are minimal [37].

Tables 4 and 5 do not contain any results for the in-plane and out-of-plane bend modes. These modes have considerably higher frequencies than the modes which are included, and they were neither accessed by our calculations, nor by the molecular beam far-infrared absorption spectra. The frequencies of these modes were recently measured for water dimers in solid Ne and p-H_2 matrices [75,76]. One should keep in mind, however, that the assignment of higher modes is not at all obvious, since the intermolecular vibrations are strongly anharmonic and also overtones and combinations of the lower modes may have considerable intensities [33]. A band that was previously assigned to the in-plane bend mode had to be reassigned to a donor torsion overtone when calculations became available [33]. Moreover, it is clear from the frequencies of modes that were measured both in molecular beams and in matrices that there are matrix shifts of 15–30 cm^{-1}. Refs. [75,76] also contains intermolecular vibrational frequencies calculated by DFT (density functional theory). Comparison of the harmonic and anharmonic frequencies from DFT calculations with the results in Tables 4 and 5 shows that the DFT results are much less accurate than ours. More in general, one may conclude that DFT calculations cannot produce water dimer potentials of the same accuracy as the CC-pol and HBB potentials described in the present paper.

We present the dimer ground state tunnelling splittings for $K=0$, 1 and 2 for H_2O and D_2O dimers with the new vibrational averaging methodology in Figs. 2 and 3,

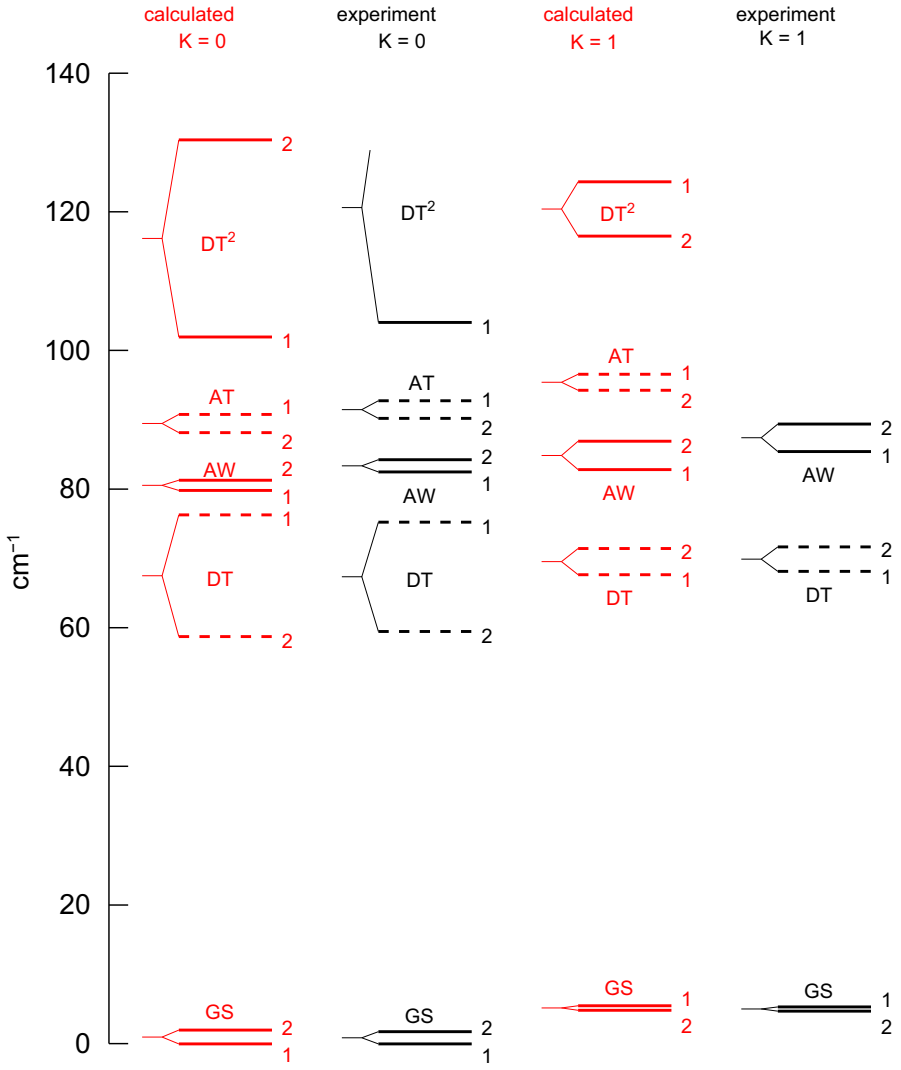

Fig. 5. VRT levels of the D_2O dimer corresponding to the intermolecular vibrations, calculated from the HBB+SHI08 potential with the vibrational averaging method, in comparison with experimental data [45]. The levels 1 and 2 are the origins, o_1 and o_2, of the A_1, E_1, B_1 and A_2, E_2, B_2 levels, respectively. The abbreviations GS, DT, AW, and AT denote the ground state (A'), donor torsion (A''), acceptor wag (A'), and acceptor twist (A'') modes [45,34]. Solid lines refer to A' symmetry, dashed lines to A'' symmetry, with respect to the point group C_s of the equilibrium structure. Note that those experimental levels which are not given have not been measured to date.

respectively, as well as other low energy states for H_2O in Fig. 4 and D_2O in Fig. 5.

It is well known that the VGS procedure gives better results than simply using the EQ geometry [71,72]. The VAP method gives a further slight improvement of the agreement with the experimental results. Our approximation to average the potential over the unperturbed monomer wavefunctions should be good for the acceptor but may be not as good for the donor molecule, since the donor OH stretch mode is significantly red-shifted by the hydrogen bond interaction [15]. However, we see that the vibrational averaging of the potential performs especially well when compared to the other methods for the GS dimer states (K=0,1).

Comparing our VAP results with the (6+6)d results of Leforestier et al., there are no large differences between them. The lower lying levels are slightly better reproduced by the latter method. However, for the higher levels the VAP results seem to produce slightly better results. A known problem with the rigid monomer approximation is that the large acceptor splitting is not represented very well: it is usually found to be much larger than the experimentally determined value. However, with the vibrational averaging technique, there is a significant improvement for both dimers. The (6+6)d method also significantly improves this feature [38].

4. Conclusion

We present a method for explicit vibrational averaging of the full dimensional water dimer potential. The dimer VRT calculations performed with the resulting vibrationally averaged potential were found to perform to the same, or slightly better, accuracy than the ground and vibrational ground state geometries in reproducing the low-lying vibration–rotation tunnelling states.

The main advantage of the approach outlined here is that it can form the basis of a method for obtaining water dimer spectra associated with excitation of the water monomers. We are particularly interested in overtone excitations which absorb at near infrared or visible wavelengths. In the present study we used monomer wavefunctions corresponding to the vibrational ground state only and G_{16} symmetry. Assuming that monomer excitations are not rapidly exchanged between the two monomers then interchange symmetry between the monomers can no longer be considered. Loss of this symmetry leads to a substantial increase in the size of the calculations. These calculations are in progress and will be reported elsewhere.

Acknowledgements

We acknowledge Xinchuan Huang, Yimin-M. Wang, Bastiaan J. Braams, and Joel M. Bowman for useful discussions and for providing us with the HBB potential. We also acknowledge useful discussion with Lorenzo Lodi, Matt Barber and Andrei Vigasin. The authors would also like to thank the NERC and EPSRC through the CAVIAR consortium for funding and also acknowledge the use of the UCL Research Computing Condor Pool and associated services in the completion of this work.

References

[1] Bukowski R, Szalewicz K, Groenenboom GC, van der Avoird A. Predictions of the properties of water from first principles. Science 2007;315:1249–52.
[2] Matsumoto M, Saito S, Ohmine I. Molecular dynamics simulation of the ice nucleation and growth process leading to water freezing. Nature 2002;416:409–13.
[3] Head-Gordon T, Hura G. Water structure from scattering experiments and simulation. Chem Rev 2002;102:2651–70.
[4] Ludwig R. Water: from clusters to the bulk. Angew Chem Int Ed 2001;40:1808–27.
[5] Stilling FH, Rahman A. Improved simulation of liquid water by molecular-dynamics. J Chem Phys 1974;60:1545–57.
[6] Liu K, Cruzan JD, Saykally RJ. Water clusters. Science 1996;271:929–33.
[7] Ugalde JM, Alkorta I, Elguero J. Water clusters: towards an understanding based on first principles of their static and dynamic properties. Angew Chem Int Ed 2000;39:717–21.
[8] Barber RJ, Tennyson J, Harris GJ, Tolchenov RN. A high-accuracy computed water line list. Mon Not R Astron Soc 2006;368:1087–94.
[9] Tinetti G, Vidal-Madjar A, Liang JP, Beaulieu MC, Yung Y, Carey S, et al. Water vapour in the atmosphere of a transiting extrasolar planet. Nature 2007;448:169–71.
[10] Ptashnik IV. Evidence for the contribution of water dimers to the near-ir water vapour self-continuum. J Quant Spectrosc Radiat Transfer 2008;109:831–52.
[11] Paynter DJ, Ptashnik IV, Shine KP, Smith KM. Pure water vapor continuum measurements between 3100 and 4400 cm^{-1}: evidence for water dimer absorption in near atmospheric conditions. Geophys Res Lett 2007;34:L12808.
[12] Ptashnik IV, Smith KM, Shine KP, Newnham DA. Laboratory measurements of water vapour continuum absorption in spectral region 5000–5600 $^{-1}$. Q J R Meteorol Soc 2004;130:2391–408.
[13] Kassi S, Macko P, Naumenkob O, Campargue A. The absorption spectrum of water near 750 nm by cw-CRDS: contribution to the search of water dimer absorption. Phys Chem Chem Phys 2005;7:2460–7.
[14] Ma Q, Tipping RH, Leforestier C. Temperature dependencies of mechanisms responsible for the water continuum absorption. I. Far wings of allowed wings. J Chem Phys 2008;128:124313.
[15] Kjaergaard HG, Low GR, Robinson TW, Howard DL. Calculated OH-stretching vibrational transitions in the water–nitrogen and water–oxygen complexes. J Phys Chem A 2002;106:8955–62.
[16] Kjaergaard HG, Robinson TW, Howard DL, Daniel JS, Headrick JE, Vaida V. Complexes of importance to the absorption of solar radiation. J Phys Chem A 2003;107:10680–6.
[17] Daniel JS, Soloman S, Kjaergaard HG, Schofield DP. Atmospheric water vapor complexes and the continuum. Geophys Res Lett 2004;31:L06118.
[18] Wang Y, Carter S, Braams BJ, Bowman JM. Multimode quantum calculations of intramolecular vibrational energies of the water dimer and trimer using ab initio-based potential energy surfaces. J Chem Phys 2008;128:071101.
[19] Kjaergaard HG, Henry BR, Wei H, Lefebvre S, Carrington T. Calculation of vibrational fundamental and overtone band intensities of H_2O. J Chem Phys 1994;100:6228–39.
[20] Low GR, Kjaergaard HG. Calculation of OH-stretching band intensities of the water dimer and trimer. J Chem Phys 1999;110:9104–15.
[21] Schofield DP, Kjaergaard HG. Calculated OH-stretching and HOH bending vibrational transitions in the water dimer. Phys Chem Chem Phys 2003;5:3100–5.
[22] Garden AL, Halonen L, Kjaergaard HG. Calculated band profiles of the OH-stretching transitions in water dimer. J Phys Chem A 2008;112:7439–47.
[23] Kjaergaard HG, Garden AL, Chaban GM, Gerber RB, Matthews DA, Stanton JF. Calculation of vibrational transition frequencies and intensities in water dimer: comparison of different vibrational approaches. J Phys Chem A 2008;112:4324–35.
[24] Hänninen V, Salmi T, Halonen L. Acceptor tunneling motion and O–H stretching vibration overtones of the water dimer. J Phys Chem A 2009;113:7133–7.
[25] Brocks G, van der Avoird A, Sutcliffe BT, Tennyson J. Quantum dynamics of non-rigid systems comprising two polyatomic fragments. Mol Phys 1983;50:1025–43.

[26] Leforestier C, Braly LB, Liu K, Elrod MJ, Saykally RJ. Fully coupled six-dimensional calculations of the water dimer vibration–rotation–tunneling states with a split Wigner pseudo spectral approach. J Chem Phys 1997;106:8527–44.

[27] Scribano Y, Leforestier C. Contribution of water dimer absorption to the millimeter and far infrared atmospheric water continuum. J Chem Phys 2007;126:234301.

[28] Huang H, Braams BJ, Bowman JM, Kelly REA, Tennyson J, Groenenboom GC, et al. New ab initio potential energy and the vibration–rotation–tunneling levels of $(H_2O)_2$ and $(D_2O)_2$. J Chem Phys 2008;128:034312.

[29] Leforestier C, Gatti F, Fellers RS, Saykally RJ. Determination of a flexible (12D) water dimer potential via direct inversion of spectroscopic data. J Chem Phys 2002;117:8710–22.

[30] Keutsch FN, Goldman N, Harker HA, Leforestier C, Saykally RJ. Complete characterization of the water dimer vibrational ground state and testing the VRT(ASP-W)III, SAPT-5st, and VRT(MCY-5f) surfaces. Mol Phys 2003;101:3477–92.

[31] Keutsch FN, Braly LB, Brown MG, Harker HA, Petersen PB, Leforestier C, et al. Water dimer hydrogen bond stretch, donor torsion overtone, and "in-plane bend" vibrations. J Chem Phys 2003;119:8927–37.

[32] Groenenboom GC, Wormer PES, van der Avoird A, Mas EM, Bukowski R, Szalewicz K. Water pair potential of near spectroscopic accuracy. II. Vibration–rotation–tunneling levels of the water dimer. J Chem Phys 2000;113:6702–15.

[33] Smit MJ, Groenenboom GC, Wormer PES, van der Avoird A, Bukowski R, Szalewicz K. Vibrations, tunneling, and transition dipole moments in the water dimer. J Phys Chem A 2001;105:6212–25.

[34] Smit MJ, Groenenboom GC, Wormer PES, van der Avoird A, Bukowski R, Szalewicz K. Vibrations, tunneling, and transition dipole moments in the water dimer. J Phys Chem A 2005;105: 6212–25.

[35] Bukowski R, Szalewicz K, Groenenboom GC, van der Avoird A. Polarizable interaction potential for water from coupled cluster calculations. I. Analysis of dimer potential energy surface. J Chem Phys 2008;128:094313.

[36] Bukowski R, Szalewicz K, Groenenboom GC, van der Avoird A. Polarizable interaction potential for water from coupled cluster calculations. II. Applications to dimer spectra, virial coefficients, and simulations of liquid water. J Chem Phys 2008;128:094314.

[37] Cencek W, Szalewicz K, Leforestier C, van Harrevelt R, van der Avoird A. An accurate analytic representation of the water pair potential. Phys Chem Chem Phys 2008;10:4716–31.

[38] Leforestier C, van Harrevelt R, van der Avoird A. Vibration–rotation–tunneling levels of the water dimer from an ab initio potential energy surface with flexible monomers. J Phys Chem A 2009;113:12285–94.

[39] Zwart E, ter Meulen JJ, Meerts WL. The submillimeter rotation tunneling spectrum of $(D_2O)_2$. Chem Phys Lett 1990;173: 115–21.

[40] Zwart E, ter Meulen JJ, Meerts WL, Coudert LH. The submillimeter rotation tunneling spectrum of the water dimer. Mol Phys 1991;147:27–39.

[41] Fraser GT. $(H_2O)_2$-spectroscopy, structure and dynamics. Int Rev Phys Chem 1991;10:189–206.

[42] Karykin EN, Fraser GT, Suenram RD. Microwave-spectrum of the K_A = 1–0 rotation–tunneling band of $(D_2O)_2$. Mol Phys 1993;78: 1179–89.

[43] Paul JB, Provencal RA, Saykally RJ. Characterization of the $(D_2O)_2$ hydrogen-bond-acceptor antisymmetric stretch by IR cavity ring-down laser absorption spectroscopy. J Phys Chem A 1998;102: 3279–83.

[44] Braly JB, Cruzan JD, Liu K, Fellers RS, Saykally RJ. Terahertz laser spectroscopy of the water dimer intermolecular vibrations. I. $(D_2O)_2$. J Chem Phys 2000;112:10293–313.

[45] Braly JB, Liu K, Brown MG, Keutsch FN, Fellers RS, Saykally RJ. Terahertz laser spectroscopy of the water dimer intermolecular vibrations. ii. $(H_2O)_2$. J Chem Phys 2000;112:10314–26.

[46] Burnham CJ, Xantheas SS. Development of transferable interaction models for water. I. Prominant features of the water dimer potential energy surface. J Chem Phys 2002;116:1479–92.

[47] Xantheas SS, Burnham CJ, Harrison RJ. Development of transferable interaction models for water. II. Accurate energetics of the first few water clusters from first principles. J Chem Phys 2002;116: 1493–9.

[48] Burnham CJ, Xantheas SS. Development of transferable interaction models for water. III. Reparametrization of an all-atom polarizable rigid model (TTMR-2) from first principles. J Chem Phys 2002;116:1500–10.

[49] Burnham CJ, Xantheas SS. Development of transferable interaction models for water. IV. A flexible, all-atom polarizable potential (TTM2-F) based on geometry dependent charges derived from an ab initio monomer dipole moment surface. J Chem Phys 2002;116:5115–24.

[50] Fanourgakis GS, Xantheas SS. Development of transferable interaction potentials for water. v. Extension of the flexible, polarizable, thole-type model potential (TTM3-F, v. 3.0) to describe the vibrational spectra of water clusters and liquid water. J Chem Phys 2008;128:074506.

[51] Huang H, Braams BJ, Bowman JM. Ab initio potential energy and dipole moment surfaces of $(H_2O)_2$. J Phys Chem A 2006;110: 445–51.

[52] Shank A, Wang Y, Kaledin A, Braams BJ, Bowman JM. Accurate ab initio and "hybrid" potential energy surfaces, intermolecular vibrational energies, and classical ir spectrum of the water dimer. J Chem Phys 2009;130:144314.

[53] Cavagnat D, Lespade L, Lapouge C. Internal dynamics contributions to the CH stretching overtone spectra of gaseous monohydrogenated nitromethane NO_2CHD_2. J Chem Phys 1995;103:10502–12.

[54] Kjaergaard HG, Rong ZM, McAlees AJ, Howard DL, Henry BR. Internal methyl rotation in the CH stretching overtone spectra of toluene-alpha-d(2), -alpha-d(1), and -d(0). J Phys Chem A 2000;104:6398–405.

[55] Partridge H, Schwenke DW. The determination of an accurate isotope dependent potential energy surface for water from extensive ab initio calculations and experimental data. J Chem Phys 1997;106:4618–39.

[56] Shirin SV, Zobov NF, Ovsyannikov RI, Polyansky OL, Tennyson J. Water line lists close to experimental accuracy using a spectroscopically determined potential energy surface for $H_2^{16}O$, $H_2^{17}O$ and $H_2^{18}O$. J Chem Phys 2008;128:224306.

[57] Shirin SV, Polyansky OL, Zobov NF, Barletta P, Tennyson J. Spectroscopically determined potential energy surface of $H_2^{16}O$ up to 25000 cm^{-1}. J Chem Phys 2003;118:2124–9.

[58] Tennyson J, Kostin MA, Barletta P, Harris GJ, Polyansky OL, Ramanlal J, et al. DVR3D: a program suite for the calculation of rotation–vibration spectra of triatomic molecules. Comput Phys Commun 2004;163:85–116.

[59] Fulton N. Physics theory. PhD thesis, University of London; 1994.

[60] Calleja M, Bruin R, Tucker MT, Dove MG, Tyer R, Blanshard L, et al. Collaborative grid infrastructure for molecular simulations: the minerals minigrid as a prototype integrated compute and data grid. Mol Sim 2005;31:303–13.

[61] Thain D, Tannenbaum T, Livny M. Distributed computing in practice: the condor experience. Concurr Comput Pract Exp 2005;17:323–56.

[62] Kain JS, Polyansky OL, Tennyson J. The ground-state potential energy surface of water: barrier to linearity and its effect on the vibration–rotation levels. Chem Phys Lett 2000;317:365–71.

[63] Tschumper GS, Leininger ML, Hoffman BC, Valeev EF, Schaefer III HF, Quack M. Anchoring the water dimer potential energy surface with explicitly correlated computations and focal point analyses. J Chem Phys 2002;116:690–701.

[64] Tennyson J, Zobov NF, Williamson R, Polyansky OL, Bernath PF. Experimental energy levels of the water molecule. J Phys Chem Ref Data 2001;30:735–831.

[65] McCoy AB, Braams BJ, Brown A, Huang X, Jin Z, Bowman JM. Ab initio diffusion monte carlo calculations of the quantum behaviour of CH_5^+ in full dimensionality. J Phys Chem A 2004;108: 4991–4.

[66] McCoy AB, Huang X, Carter S, Landeweer MY, Bowman JM. Full-dimensional vibrational calculations for $H_5O_2^+$ using an ab initio potential energy surface. J Chem Phys 2005;122:061101.

[67] Anderson JA. A random-walk simulation of the Schrodinger equation. J Chem Phys 1975;63:1499–503.

[68] Anderson JA. Quantum chemistry by random walk. H_2^+, H_3^+ D_{3h} $^1A'^1$, H_2 $^3\sigma_u^+$, H_4 $^1\sigma_g^+$, Be ^1S. J Chem Phys 1976;65:4121–7.

[69] Suhm MA, Watts RO. Quantum Monte Carlo studies of vibrational states in molecules and clusters. Phys Rep 1991;204:293–329.

[70] Kosztin I, Faber B, Schulten K. Introduction to the diffusion Monte Carlo method. Am J Phys 1996;64:633–44.

[71] Mas EM, Szalewicz K. Effects of monomer geometry and basis set saturation on computed depth of water dimer potential. J Chem Phys 1996;104:7606–14.

[72] Jeziorska M, Jankowski P, Szalewicz K, Jeziorski B. On the optimal choice of monomer geometry in calculations of intermolecular

interaction energies: rovibrational spectrum of ArHF from two- and three-dimensional potentials. J Chem Phys 2000;113:2957–68.
[73] Csaszar AG, Czako G, Furtenbacher T, Tennyson J, Szalay V, Shirin SV, et al. On equilibrium structures of the water molecule. J Chem Phys 2005;122:214305.
[74] Zobov NF, Shirin SV, Polyansky OL, Tennyson J, Coheur P-F, Bernath PF, et al. Monodromy in the water molecule. Chem Phys Lett 2005;414:193–7.
[75] Ceponkus J, Uvdal P, Nelander B. Far-infrared band strengths in the water dimer: experiments and calculations. J Phys Chem A 2008;112:3921–6.
[76] Ceponkus J, Uvdal P, Nelander B. Intermolecular vibrations of different isotopologs of the water dimer: experiments and density functional theory calculations. J Chem Phys 2008;129: 194306.